

We are IntechOpen, the world's leading publisher of Open Access books Built by scientists, for scientists

6,900

Open access books available

185,000

International authors and editors

200M

Downloads

Our authors are among the

154

Countries delivered to

TOP 1%

most cited scientists

12.2%

Contributors from top 500 universities



WEB OF SCIENCE™

Selection of our books indexed in the Book Citation Index
in Web of Science™ Core Collection (BKCI)

Interested in publishing with us?
Contact book.department@intechopen.com

Numbers displayed above are based on latest data collected.
For more information visit www.intechopen.com



GaN Based Ultraviolet Photodetectors

D. G. Zhao and D. S. Jiang

*State Key Laboratory on Integrated Optoelectronics,
Institute of Semiconductors, Chinese Academy
of Sciences, Beijing
P. R. China*

1. Introduction

The band gaps of the III-nitrides are large and direct, which are 0.7 eV for InN, 3.4 eV for GaN, and 6.2 eV for AlN (Jain et al., 2000; Wu et al., 2002), consequently There are many areas where conventional semiconductors including Si and GaAs cannot be used. For example, short wavelength light emitters are required for full color display, high density information storage, and under water communication. However, III-nitrides are particularly suitable for applications in these areas. A great success in device applications has been obtained so far, including the realization of high brightness blue GaN based light emitting diodes (LED) and long lifetime GaN based laser diodes (LD) (Nakamura, 1998).

On the other hand, III-nitrides are one of the most promising materials for the fabrication of high-sensitivity visible-blind ($\lambda \leq 365\text{nm}$) and solar-blind ($\lambda \leq 280\text{nm}$) ultraviolet (UV) photodetectors, which have extensive applications in flame detection, secure space-to-space communication, and ozone layer monitoring. Various types of GaN-based photodetectors have been realized, including p-i-n and Schottky barrier photodetectors, solar-blind ultraviolet photodetector focal plane arrays, and UV avalanche photodiodes (McClintock et al., 2005; Zhao et al. 2007a; Cicek et al., 2010). The fabrication of GaN-based photodetectors were reviewed in some articles previously (Muñoz et al., 2001). Since the quality of GaN materials plays a key role in determining the performance of GaN UV photodetectors, in this chapter, firstly the growth and properties of GaN materials are introduced, then the device technology and fabrication are presented, finally a conclusion is drawn.

2. GaN material growth and ultraviolet photodetector's fabrication

The GaN-based materials used for device applications investigated in this chapter are grown on the c-plane sapphire substrate by metalorganic chemical vapor deposition (MOCVD). The ammonia (NH_3), trimethylgallium (TMGa), trimethylaluminum (TMAI) and Silane (SiH_4) have been used as N, Ga, Al, and Si precursors, respectively. H_2 has been used as the carrier gas. The quality of the thin films is mainly characterized by the double x-ray diffraction (DCXRD) and photoluminescence (PL). The full width at half maximum (FWHM) of DCXRD ω -scan rocking curves is obtained using a Rigaku SLX-1AL x-ray diffractometer. A 325 nm He-Cd laser is employed as excitation light in the measurement of the PL spectra.

2.1 Material growth for GaN based UV photodetectors

Many attempts were made to synthesize GaN crystals during the period 1930–1960, but good quality crystals could not be grown for a long period of time, mainly because there are large lattice mismatch and thermal mismatch between the III-nitrides and widely-used heteroepitaxial substrates (Jain et al., 2000). The beginning of the growth of good quality epilayers was made by the two-step method (Amano et al., 1986; Nakamura, 1991). In the following, we will firstly introduce the MOCVD growth of GaN epilayers, then the AlGaN growth will be discussed with the parasitic reaction between the TMAI and NH_3 in MOCVD, finally the defects and related yellow luminescence of GaN films are studied.

2.1.1 GaN material growth using the two-step method

The two-step growth method of GaN epilayer with low-temperature AlN buffer layers by MOCVD is studied. (Zhao et al., 2004). The growth procedure is as follows: Firstly the AlN buffer layer is grown on sapphire substrate at 600°C and annealed in a temperature ramp, then a GaN epilayer about 2.5 μm thick is deposited on the AlN buffer layer at 1080°C. The real-time *in situ* optical reflectivity measurements are employed to monitor the whole growth stages of GaN materials.

Fig. 1 shows the traces of *in situ* optical reflectivity measured from the two GaN epilayers samples A and B grown on a 20 nm thick AlN buffer layer with different annealing processes during the temperature elevation after the growth of low-temperature AlN buffer layer. The annealing time of AlN buffer layer used in the growth of two samples A and B are 1000 second and 300 second, respectively. In Fig. 1(a) and (b), two traces are divided into three parts corresponding to three growth stages of GaN deposit on low-temperature AlN buffer layer as follows: (i) the low-temperature AlN buffer layer deposition, (ii) temperature ramp and anneal of the AlN buffer layer, (iii) the growth of GaN epilayers. The differences in the surface evolution processes during the growth of samples A and B are observed. In the initial growth stage of sample A where GaN epilayer is deposited on AlN buffer layer with a 1000 second annealing time, the surface of GaN layer becomes rough and the intensity of the *in situ* optical reflectivity decreases, then the surface of GaN layer turns to be optically smoother step by step, it means the lateral growth and coalescence of GaN islands emerge (Han et al., 1997), at last the quasi two-dimensional growth of GaN layer occurs. An oscillation of the reflectivity intensity with large and equal amplitude is well observed. However, the growth procedures of sample B deposited on AlN buffer layer with a 300 second annealing time shows a different kind of trace in Fig. 1(b). The surface roughing of GaN islands does not clearly appear. There is nearly no change in the intensity of *in situ* optical reflectivity during the starting period of the growth of GaN epilayer, as shown by the arrow in Fig. 1(b). As shown in Table 1, sample A has a narrower FWHM of x-ray rocking curve and a higher electron mobility, it seems that the longer annealing time of low-temperature AlN buffer layer tends to promote a lateral growth of GaN islands, and the quality of GaN epilayers is improved. It also suggests that the lateral growth of GaN islands is helpful to decrease the edge threading dislocations, since the FWHM of x-ray ω -scan rocking curve for (0002) and (10-12) planes represents indirectly the density of screw and edge threading dislocations (Heying et al., 1996; Heinke et al., 2000).

Samples	AlN Buffer layer		XRD FWHM (arcmin)		Electron Mobility (cm ² /Vs)
	Annealing Time (s)	Thickness (nm)	(0002)	(10-12)	
A , E	1000	20	6.9	11.2	360
B	300	20	8.1	19.1	142
C	1000	45	10.2	28.6	73
D	1000	30	7.2	13.9	217
F	1000	16

Table 1. Growth condition and characterization result of GaN samples.

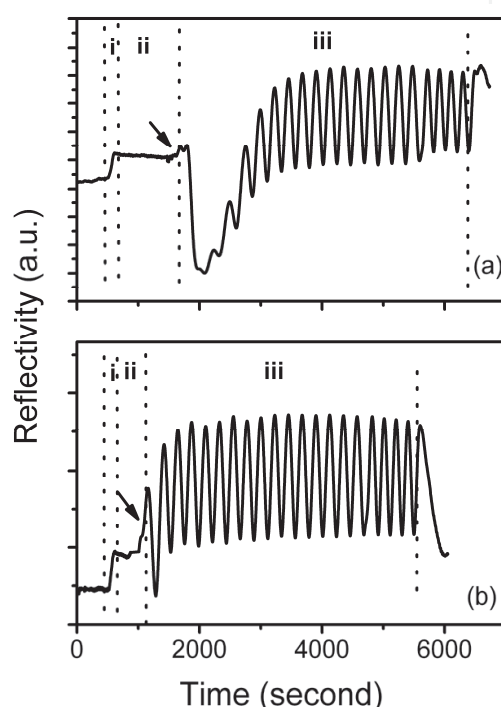


Fig. 1. The traces of *in situ* optical reflectivity measurements for the three stages in the whole growth process of GaN epilayers on low-temperature AlN buffer layer with different annealing time: (a) 1000 s (b) 300 s.

It is found that not only the annealing time, but also the thickness of low-temperature AlN buffer layer has an enormous influence on the quality of GaN epilayers. The traces of *in situ* optical reflectivity measured from GaN epilayers growth on low-temperature AlN buffer layer with different thickness are shown in Fig. 2(a)-(d), where the dashed lines denote the start of GaN epilayers growth. For the four samples, the same 1000 second annealing time of low-temperature-grown AlN is employed but the thickness of low-temperature AlN buffer layer is different. They are 45nm, 30nm, 20nm, and 16nm for sample C, D, E (where sample E and sample A is the same sample with different names) and F, respectively. It can be seen from Fig. 2 that there exist a lot of differences in the reflectivity curves measured during the initial stage of the growth process of GaN epilayers. Nearly no any growth of GaN islands (surface roughing process in the initial growth stage) and their coalescence (lateral growth) is observed in the starting period of growth process of sample C which is deposited on the 45 nm AlN buffer layer. There is a little growth of GaN islands and their coalescence in the

growth process of sample D which is deposited on the 30 nm AlN buffer layer. With thinner AlN buffer layer, however, the obvious lateral growth of GaN islands is observed in the growth process for sample E, as shown in Fig. 2 (c). The growth process of sample F is stopped as shown in Fig. 2(d), indicating that the AlN buffer layer is too thin to lead to the coalescence of GaN islands and to start a quasi two-dimensional growth. In this case the quality of GaN epilayers becomes very bad. As shown in Table 1, the optimal thickness of AlN buffer layer in this growth condition is around 20nm. A too thick or too thin AlN buffer layer will lead to the deteriorated quality of GaN epilayers.

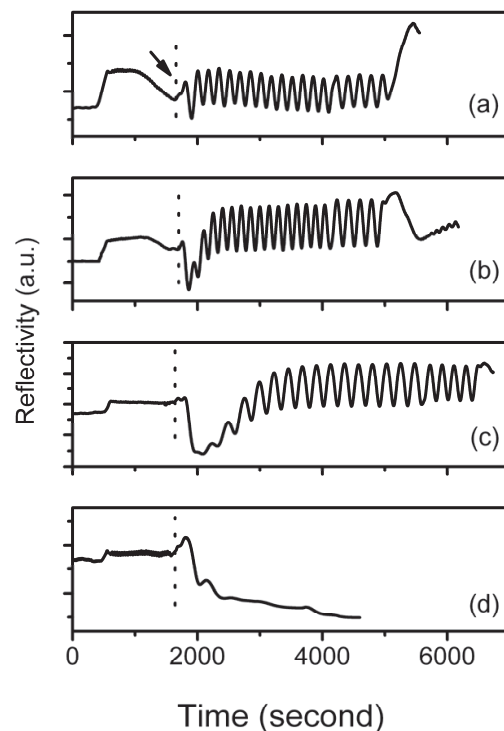


Fig. 2. The traces of in situ optical reflectivity measurements for the whole growth process of GaN epilayers on low-temperature AlN buffer layer with the same 1000 s annealing time and different thickness: (a) 45 nm, (b) 30 nm, (c) 20 nm, (d) 16 nm. The dashed lines denote the start of GaN epilayer's growth.

In order to gain further insight to the effect of AlN buffer layer on the quality of GaN layers, three AlN buffer layers *a*, *b*, and *c* with growth stopped just before the growth of high temperature GaN epilayers [indicated by arrow in Fig. 1(a), (b) and Fig. 2(a)] are prepared and examined by atomic force microscopy (AFM). These AlN buffer layers are grown under the same growth conditions as those in samples A, B, and C, i.e. *a* (1000 second annealing, 20nm thickness), *b* (300 second annealing, 20nm thickness), and *c* (1000 second annealing, 45nm thickness), respectively. The surface morphology of these AlN buffer layers is shown in Fig. 3(a), (b) and (c), respectively. They are quite different, and the sample *a* has the largest grain size and the lowest nuclei density as shown in Fig. 3. It is known that the GaN epilayer A which is grown on the AlN buffer layer *a* has the best quality, implying that the quality of GaN epilayers is closely related to the surface morphology of AlN buffer layer. Because the GaN islands in the initial growth stage will coalesce quickly if the AlN buffer layer has small grain size and high nuclei density, as a result, a lot of formed dislocations will go through the GaN epilayers, leading to a deteriorated quality. On the

other hand, the quality of GaN epilayers deposit on AlN buffer layer with large grain size and low nuclei density will be much better, since the lateral growth and coalescence of GaN islands will be prolonged, which leads to an increased volume of defect-free columnar domains and improve the crystal quality (Han et al., 1997). Of course, when the AlN buffer layer has too large grain size and too low nuclei density, it will take a too long time for the lateral growth of GaN islands, the quality of GaN epilayers will also become bad. Therefore, it is concluded that the quality of GaN epilayers is dependent on the grain size and the nuclei density of AlN buffer layer. A long time annealing and a suitable thickness of AlN buffer layer are very important to the growth of high quality GaN epilayers.

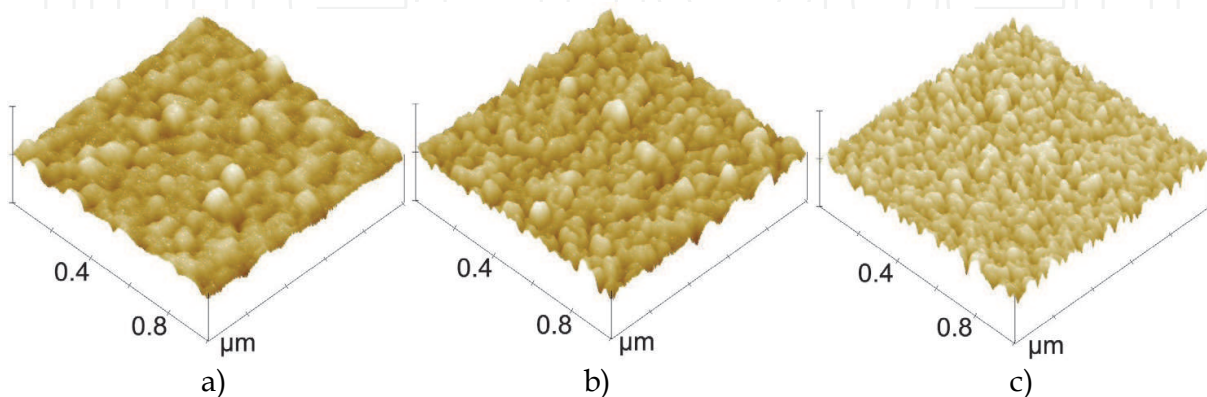


Fig. 3. AFM images of the surface morphology of the AlN buffer layers, where a, b, and c are for the growth of samples A, B, and C, respectively

Besides the growth condition of low-temperature AlN buffer layer, the V/III ratio in the initial growth stage has an important influence on the quality of a GaN epilayer grown by MOCVD, and the quality of GaN epilayer could be improved by employing a lower V/III ratio in the initial growth stage and intentionally prolonging the island coalescence process (Zhao et al., 2007b, 2009a). After optimizing the growth conditions, high-mobility MOCVD-grown n-type GaN films of about 4 μm in thickness were reported (Zhao et al., 2006a). The electron mobility at room temperature was as high as 1005 cm^2/Vs at an electron concentration of $1.1 \times 10^{16} \text{ cm}^{-3}$. Fig. 4 shows the Hall measurement results of high quality GaN samples. This is one of the best values reported for GaN films grown by MOCVD.

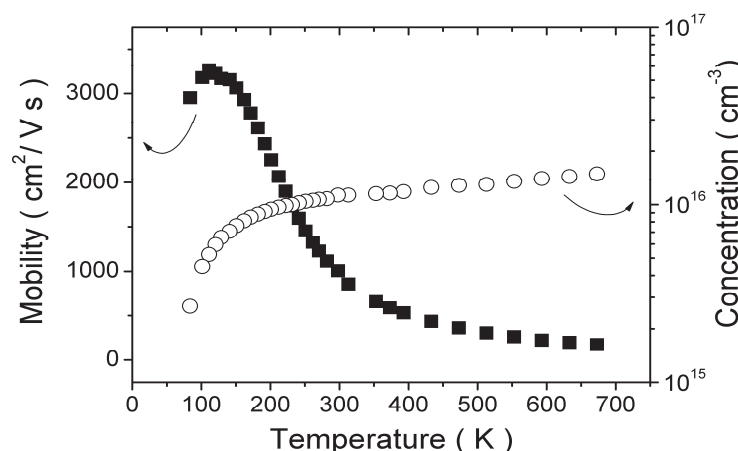
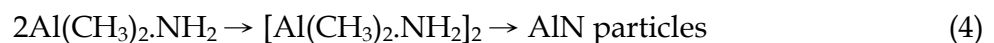
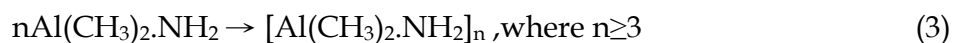
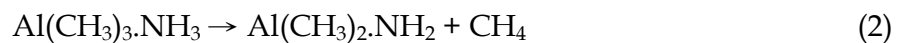


Fig. 4. The temperature-dependent electron mobility (solid square) and concentration (open circle) of high quality n-type GaN sample. The electron mobility at room temperature was as high as 1005 cm^2/Vs at an electron concentration of $1.1 \times 10^{16} \text{ cm}^{-3}$.

2.1.2 Parasitic reaction between TMAI and NH₃ in MOCVD

AlGa_{1-x}N materials are important for producing solar-blind ultraviolet photodetectors. However, the parasitic reaction of TMAI and NH₃ occurring in the vapor phase is much more serious than that of TMGa and NH₃ (Mihopoulos et al, 1998), and it has an important influence on the growth of AlGa_{1-x}N materials. We will discuss parasitic reaction of TMAI and NH₃ in MOCVD and study how to reduce its effect in this section (Zhao et al., 2006b).

Fig. 5 shows the relationship between the growth rate of AlN at different reactor pressure of 50, 200 and 500 Torr in MOCVD system, respectively. It is found that with the increase of growth temperature, the growth rate of AlN increase slowly when the reactor pressure is as small as 50 Torr, while it instead decreases with increasing growth temperature if the reactor pressure is raised to 200 Torr, and it decreases even more rapidly if the reactor pressure is 500 Torr. Usually it is difficult to grow AlN material at low temperature because of the difficulty of decomposing NH₃. However, the growth rate of AlN at high growth temperature is much slower than at low temperature when a relatively high reactor pressure is adopted during the growth. Such abnormal growth rate dependence on growth temperature is attributed to the parasitic effect of NH₃ and TMAI. It is known that there is a boundary layer above the substrate in the reaction chamber, and the gas precursors have a residence time in the MOCVD process. The process related to parasitic reaction of TMAI and NH₃ in the vapor phase can be described as follows (Mihopoulos et al, 1998),



During the growth, the AlN particles formed by parasitic reaction according to the equation (4) and (5) are carried away from the deposition zone and do not contribute to the growth (Mihopoulos et al, 1998). It is reported that the dimers (i.e. $[\text{Al}(\text{CH}_3)_2 \cdot \text{NH}_2]_2$) have sufficient energy to lose methyl groups to form AlN particles at high temperature (Mihopoulos et al, 1998). Therefore, if parasitic reaction plays an important role, much more AlN particles will be engendered with the increase of growth temperature, and the growth rate of AlN will decrease. Such effect is significant under a high reactor pressure. However when the reactor pressure is as low as 50 Torr, the surface kinetically-limited mechanism is competed with the gas phase parasitic reaction and becomes dominated, the growth rate of AlN is expected to increase with the growth temperature as is expected. From the experimental result it is deduced that the parasitic reaction depends on the reactor pressure besides the growth temperature, i.e. it dominates when the reactor pressure is 200 Torr and 500 Torr, and is less significant at 50 Torr. It is reasonable that the chance for TMAI and NH₃ to come into contact increases at higher reactor pressures, and the formation of trimers (i.e. $[\text{Al}(\text{CH}_3)_2 \cdot \text{NH}_2]_3$) and higher n-mers($[\text{Al}(\text{CH}_3)_2 \cdot \text{NH}_2]_n$ for $n > 3$) is enhanced by the increasing reactor pressure, as a result, the parasitic reaction between TMAI and NH₃ becomes weak at a low reactor pressure.

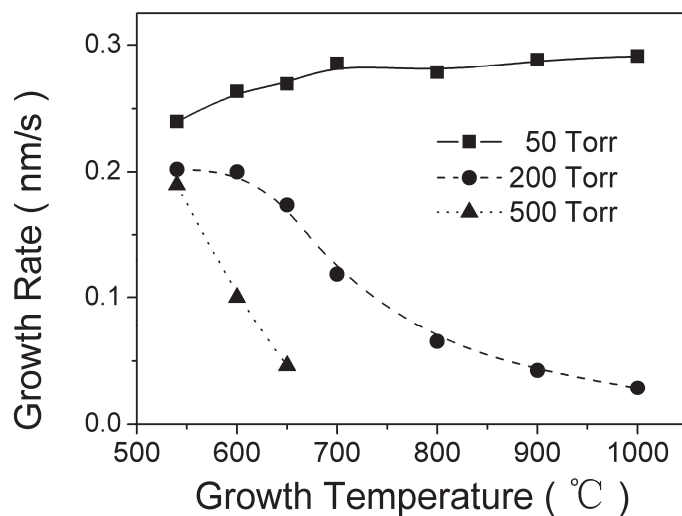


Fig. 5. The measured growth rate of AlN versus the growth temperature, the reactor pressures adopted in the growth are 50, 200 and 500 Torr, respectively.

The dependence of the AlN growth rate on the flux of NH_3 is also studied, and a very interesting phenomena are observed as shown in Fig. 6. It is found that whatever the other growth parameters are taken, the growth rate of AlN always decreases with the increase of the flux of NH_3 in the range shown in Fig. 6. The parasitic reaction is expected to be responsible for the phenomena. It has been reported that NH_3 can reduce the potential energy barrier of trimers and higher n-mers formation (Nakamura et al., 2000). Therefore, with the increase of the flux of NH_3 , the quantities of trimers and higher n-mers which do not contribute to the growth will increase, and the growth rate of AlN will decrease. It is found that the growth temperature has an effect on the changing speed of growth rate with increasing flux of NH_3 . The data measured at 800 °C and 540 °C are denoted by squares and circles respectively in Fig.6. It can be seen that the growth rate of AlN decreases rapidly at higher growth temperature, which supports the conclusion that higher growth temperature enhances parasitic reaction as suggested by the result of Fig. 5. In addition, with the increase of the flux of NH_3 , parasitic reaction is enhanced at higher growth temperature, therefore the growth rate of AlN decreases rapidly. On the other hand, the variation of the growth rate with respect to the flux of NH_3 is also influenced strongly by the reactor pressure, as shown by the two curves in the lower part of Fig. 6 which are measured at the flux of 500 Torr and 50 Torr, respectively. It indicates that at a higher reactor pressure, more trimers and higher n-mers are formed with the increase of NH_3 flux due to parasitic reaction. As a result, the growth rate of AlN decreases more rapidly with the increase of NH_3 flux. Taking the above result into account, it is concluded that the parasitic reaction can be reduced by decreasing the growth temperature, reactor pressure and the flux of NH_3 .

The further research results confirm that low reactor pressure can weaken parasitic reactions and lead to a higher Al content in AlGaIn film (Deng et al., 2011). On the other hand, the enhancement of the surface mobility of Al is especially important for high quality AlGaIn layers (Zhao et al., 2006b, 2008a). The migration-enhanced MOCVD is intended to carry on for improving the surface dynamic behavior of Al atoms in the growth (Zhang et al., 2002).

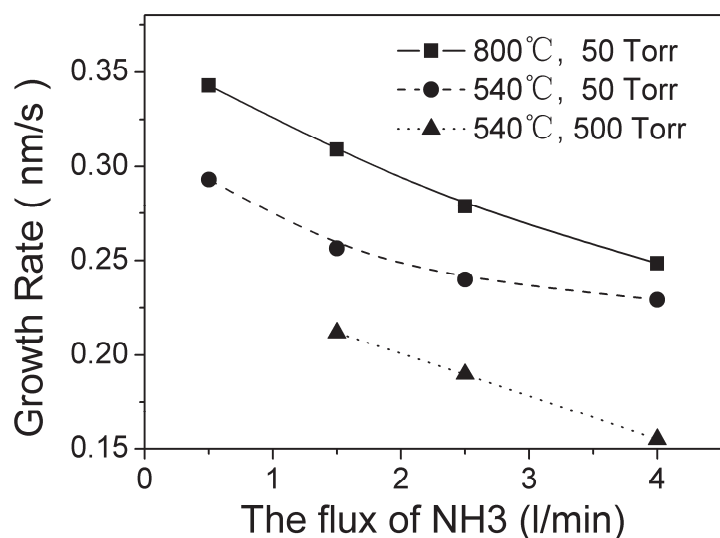


Fig. 6. The measured growth rate of AlN versus the flux of NH₃. Either the growth temperature or reactor pressure are different for the three curves.

2.1.3 Yellow luminescence and related defects in GaN materials

There are many problems of GaN materials are still hung in controversy till now. It is well-known that there is a yellow luminescence band centered at 2.2–2.3eV in the PL spectra of GaN. The mechanism behind it is still under disputation (For example, see Reshchikov & Morkoc, 2005). We find that the edge dislocations play an important role in enhancing the yellow luminescence of n-type GaN samples (Zhao et al.,2006d).

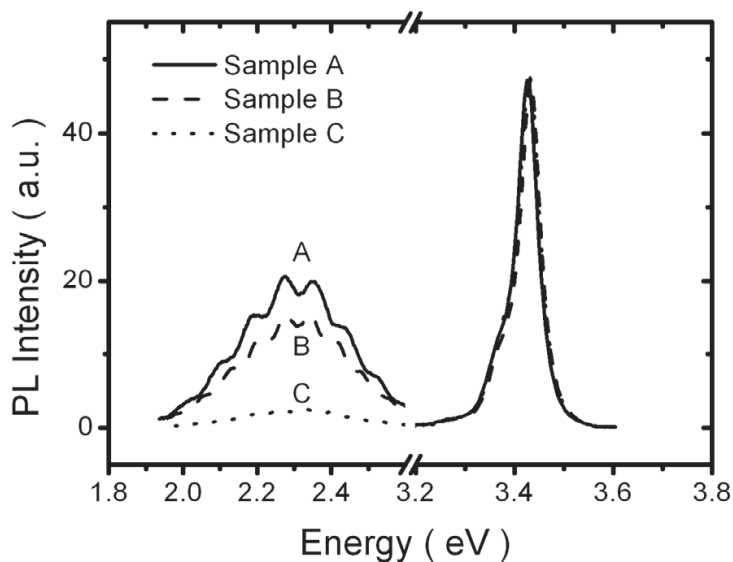


Fig. 7. Room temperature PL spectra of GaN samples A, B, and C of series I, which have the same Si doping, where the intensity of the near-band-edge luminescence peak at 3.42 eV is normalized.

Two series of GaN samples were prepared in our experiment. There were ten GaN samples in series I, where different growth conditions were used but the same SiH₄ flux of 0.72 nmol/min was employed during the materials growth. Fig. 7 shows the room

temperature(RT) PL spectra of three typical samples, A, B, and C in this series. The DCXRD characterization results of these three samples are listed in Table 2. As shown in Fig. 7, the broad band centered at 2.3 eV is the yellow luminescence. The undulations of the yellow luminescence band are formed by light interference. The intensity of the near-band-edge luminescence peak at 3.42 eV is normalized for the three PL spectra in Fig. 7. The integrated intensity ratios of the yellow luminescence band to the near-band-edge emission (I_{YL}/I_{BE}) are 2.14, 1.20, and 0.27 for samples A, B, and C, respectively. As shown in Table 2, sample A has the widest DCXRD FWHM at the (102) plane, and sample C has the narrowest DCXRD FWHM at the (102) plane. Correspondingly, sample A has the most intense yellow luminescence band, while sample C has the least. The relative intensity of yellow luminescence band seems to be strongly dependent on the FWHM at the (102) plane.

The solid square symbols in Fig. 8 show the dependence of the I_{YL}/I_{BE} value on the DCXRD FWHM at the (102) plane for the all ten samples of series I. The figure clearly indicates that the relative intensity of the yellow luminescence band increases as the DCXRD FWHM at the (102) plane increases. However, we have also found that the relative intensity of yellow luminescence exhibits a random fluctuation when the DCXRD FWHM at the (002) plane increases (not shown here). It has been reported that the GaN samples with narrower DCXRD FWHM at the (002) plane have lower screw dislocation densities, while the GaN samples with narrower FWHM at the (102) plane have lower edge dislocation densities (Heying et al., 1996; Heinke et al., 2000). Therefore, the above-mentioned results suggest that the intensity of the yellow luminescence band in n-type GaN is not influenced by the density of screw dislocations, but is strongly related to the edge dislocations.

Sample	DCXRD FWHM (arcsec)		SiH ₄ Flux (nmol/min)	n (cm ⁻³)	I_{YL}/I_{BE} (a.u.)
	(002)	(102)			
A	428	835	0.72	8.8×10^{16}	2.14
B	382	605	0.72	2.1×10^{17}	1.20
C	425	490	0.72	2.6×10^{17}	0.27

Table 2. Characterization results and Si doping condition of n-type GaN samples in series I

Hall measurements were carried out to gain further insight into the behavior of edge dislocations in GaN. Fig. 8 shows the dependence of net carrier concentration of the n-type GaN samples of series I (hollow triangle symbols) on the DCXRD FWHM at the (102) plane. We observed that the carrier concentration decreased with the increase of the FWHM at the (102) plane. This is surprising because the same Si doping is used during the growth of this series of GaN samples. This implies that edge dislocations may influence the net carrier concentration of GaN samples. It is well known that there are many dangling bonds along the edge dislocation lines, and they can introduce deep acceptor centers which may capture electrons from the conduction band in n-type semiconductors (Read, 1954; Podor, 1966). It has been proved that the negatively charged acceptors introduced by the dislocation line act as scattering centers in n-type GaN (Ng et al., 1998; Look & Sizelove, 1999). Therefore, the decrease of free electron concentration shown in Fig. 8 can be attributed to the compensation effect from the increasing acceptor levels introduced by the edge dislocations. This result confirms that the edge dislocations introduce acceptors in n-type GaN samples.

It is widely accepted that the yellow luminescence is caused by the transition of donor-acceptor (DA) pairs (For example, Reshchikov & Morkoc, 2005). The average distance

between donors and acceptors plays a key role in determining the luminescence efficiency of the radiative recombination in the yellow luminescence band. It is found that there are many positively charged donors surrounding the negatively charged edge dislocation core in Si-doped GaN (Krtschil et al., 2003). The transition probability of electrons and holes between donors and acceptors will be higher around edge dislocations as the average distance of DA pairs becomes shorter and the overlap integral between electron and hole wavefunctions becomes larger, which will lead to an enhancement of the luminescence efficiency of the yellow band by the edge dislocations.

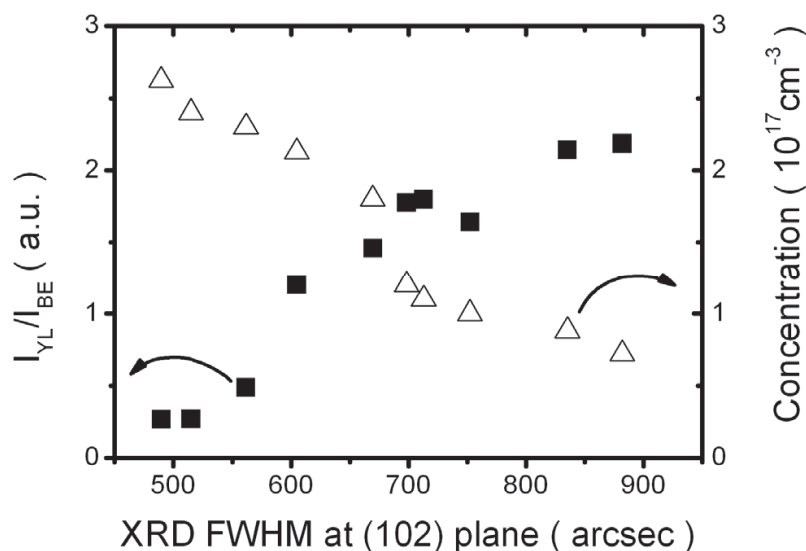


Fig. 8. The ratio between integrated intensity of the yellow luminescence band to near-band-edge emission (I_{YL}/I_{BE}) (solid squares) and the net carrier concentration (hollow triangles) vs. DCXRD FWHM at the (102) plane for the ten GaN samples of series I.

In order to study the source of donor species involved in the yellow luminescence, a different Si doping experiment was performed in which the series II GaN samples were studied. The structural quality of the series II GaN samples was high, the DCXRD FWHM at the (002) and (102) planes of these samples as narrow as 180 arcsec was obtained. Fig. 9 shows the PL spectra of samples D, E, F, and G, for which the SiH_4 fluxes used during MOCVD growth were 0, 0.05, 0.22, and 0.45 nmol/min, respectively. The corresponding electron concentrations are $5.0 \times 10^{15} \text{ cm}^{-3}$, $1.5 \times 10^{16} \text{ cm}^{-3}$, $8.8 \times 10^{16} \text{ cm}^{-3}$, and $1.8 \times 10^{17} \text{ cm}^{-3}$, respectively. In Fig. 9, the PL intensity is normalized according to the intensity of the near-band-edge emission. The ratio I_{YL}/I_{BE} increases as the SiH_4 flux increases, which is 0.15, 0.23, 0.32, and 0.35 for samples D, E, F, and G, respectively. It is well known that Si impurity atoms act as shallow donors in GaN and can increase the electron concentration in GaN samples. The PL results indicate that Si impurity has an influence on the relative intensity of the yellow luminescence band. This is reasonable if the Si donors are involved in the yellow luminescence in n-type GaN as a component of the related donor-acceptor pairs, although the multiple origins of the yellow luminescence are proved to co-exist (For example, Reshchikov & Morkoc, 2005). Due to the high quality of the GaN samples of series II which have a very low background carrier concentration as small as $5.0 \times 10^{15} \text{ cm}^{-3}$ for the unintentionally-doped GaN and a low dislocation density, a better observation of the correlation between Si doping and relative intensity of the yellow luminescence in these Si-

doped samples becomes possible. For example, as shown in the insets of Fig. 9, the PL spectrum of sample G measured at 10K demonstrates a sharp peak of donor-bound exciton luminescence at the energy of 3.490eV with an FWHM as narrow as 1.6 meV.

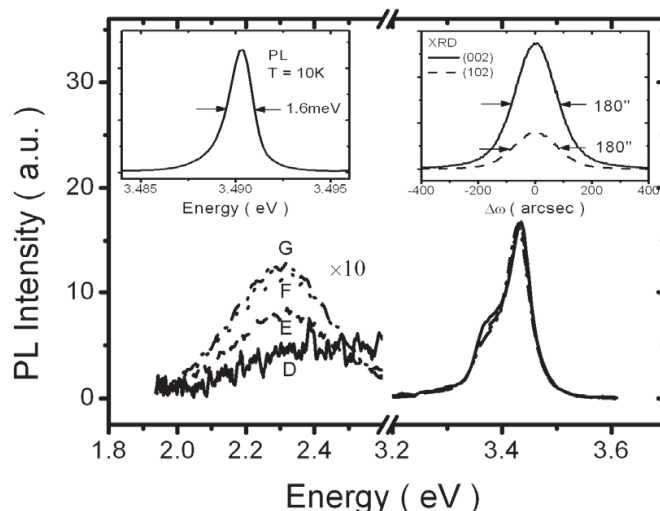


Fig. 9. RT PL spectra of GaN samples D, E, F, and G in series II with different Si doping, which have the same DCXRD FWHM at the (102) plane as narrow as 180 arcsec. In the figure the intensity of the near-band-edge luminescence peak at 3.42 eV is normalized. The insets are the ω -scan rocking curve of DCXRD(right) and 10K PL spectrum(left) of sample G.

The above results suggest that the yellow luminescence is effectively enhanced by the DA pair transitions from donor impurities such as Si to acceptors around the edge dislocations in n-type GaN. It is also found that the edge dislocation and Si impurity play important roles in linking the blue and yellow luminescence bands in n-type GaN films (Zhao et al., 2009b). In addition, there is some relationship between the yellow luminescence band and electron mobility of n-type GaN, but it is not a simple one (Zhao et al., 2007c). In fact, even the intensity of yellow luminescence is often used as an indicator of material quality for GaN, it does not have any monotonous correlation with the electron mobility of GaN.

2.2 Fabrication of GaN based UV photodetectors

On the basis of material growth, the fabrication of GaN based UV photodetectors are studied. Firstly the relationship between defects and performance of Schottky barrier photodetectors is investigated, then the fabrication of p-i-n high performance UV avalanche photodiodes are introduced, finally some new GaN photodetector devices are proposed.

2.2.3 Influence of defects on the responsivity of GaN Schottky barrier UV photodetectors

In this section, the effect of defects on the responsivity of GaN Schottky barrier UV photodetectors is investigated (Zhao et al., 2007a). A schematic diagram of the Schottky barrier photodetector structure is shown in Fig. 11. The top transparent Schottky barrier was formed on the n^- -GaN layer using Ni/Au (3nm/3nm) metal film, and the bottom Ohmic contact to the n^+ -GaN layer was made with Ti/Al/Ti/Au metal. Table 3 lists the carrier concentration in the n^- -GaN layer and the DCXRD FWHM of three samples A, B, and C.

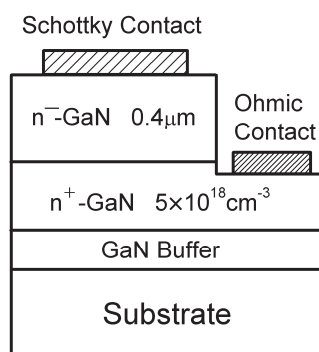


Fig. 10. Schematic diagram of GaN Schottky barrier ultraviolet photodetectors

Samples No.	FWHM of DCXRD (arcsec)		n ⁻ -GaN Layer
	(002)	(102)	
A	190	195	Si-doped, $n \approx 1.6 \times 10^{16} \text{cm}^{-3}$
B	290	320	Si-doped, $n \approx 1.0 \times 10^{17} \text{cm}^{-3}$
C	230	245	undoped, $n \approx 2.0 \times 10^{16} \text{cm}^{-3}$

Table 3. The main difference in the structure parameters and epilayer XRD characterization result of three photodetector samples

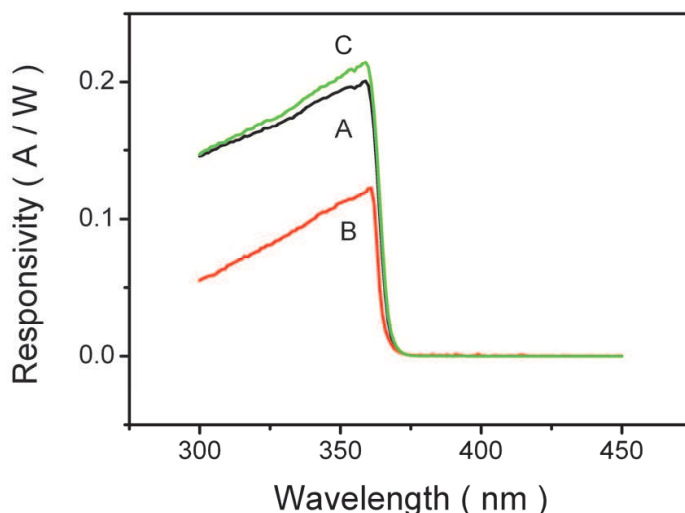


Fig. 11. The zero bias spectral response of Schottky barrier photodetector samples A, B and C (See text), where sample C uses undoped GaN layer as n⁻-GaN layer, samples A and B use lightly Si-doped ones .

We have investigated photocurrent spectra of many Schottky barrier photodetectors with different n⁻-GaN/n⁺-GaN structure. Most of them show a high responsivity near the band edge of GaN, which decreases with increasing photon energy due to the reduction of penetration depth of light and the increase in surface recombination of photogenerated carriers. Fig. 11 depicts the spectral response at zero bias for three typical ultraviolet photodetector samples, A, B and C. The n⁻-GaN layers in samples A and B are doped with Si, but have different carrier concentrations n and DCXRD FWHM values, as shown in Table 3. The peak responsivity is

about 0.20, 0.12 and 0.21 A/W for samples A, B, and C, respectively. Considering the n^- -GaN layers of sample A and B are both Si-doped, we firstly investigated the mechanism behind the different responsivity for these two photodetectors. After the device simulation, it is confirmed that the difference in the electron concentration can not be mainly responsible for the difference in responsivity between these two Schottky photodetectors (Zhao et al., 2007a). Actually, sample B has a higher dislocation density as shown by the DCXRD FWHM and a lower responsivity, indicating that dislocations can play a role in decreasing the responsivity of GaN photodetector. A lot of research work have discussed the behavior of dislocations in GaN, and they have confirmed that the dislocation cores are normally negatively charged in n-type GaN (Krtschil et al., 2003). It is reasonable to conceive that dislocation-induced acceptor levels can increase the recombination probability of photogenerated electron-hole pairs and thus reduce the responsivity of GaN ultraviolet photodetectors (Zhao et al., 2006d). Therefore, normally the responsivity of GaN based photodetectors can be improved through decreasing the dislocation density of the epilayer structure.

It is noted that the properties of different kinds of n^- -GaN layer, i.e., undoped or Si-doped, may cause a difference in the responsivity of GaN Schottky barrier photodetectors. Fig. 13 shows a comparison of the spectral responses between samples A and C, where the n^- -GaN layer of sample C is not Si-doped. Compared with sample A, sample C shows an unexpectedly higher peak responsivity of 0.21 A/W even though it has a higher dislocation density. It suggests that the major difference between the two samples is caused by the Si doping of n^- -GaN layer. The positron annihilation experiment has confirmed that the lightly Si doping can increase the concentration of Ga vacancies in comparison with undoped n-type GaN, and lead to a decrease in the minority carrier diffusion length (Zhao et al., 2006e). It is thus proposed that the photo-generated holes can be trapped by the Ga vacancies. The n^- -GaN layer in sample C has a lower concentration of Ga vacancies than in samples A and B. Since the photocurrent in the investigated Schottky barrier photodetector mainly comes from the drift current, the concentration of movable photogenerated holes in the depletion region has a strong influence on the photocurrent. The Ga vacancies will trap photogenerated carriers and increase their recombination probability in the depletion region, leading to a serious reduction of responsivity. The Ga vacancies may play an important role in the reduction of responsivity of GaN Schottky barrier photodetectors. It is also found that the Ga vacancies may lead to an increase of leakage current of GaN Schottky barrier photodetectors (Zhao et al., 2010a). Of course, it is also possible that other defects such as Ga vacancies complexes or unknown defects due to the Si doping will increase the recombination of photogenerated electron-hole pairs and reduce the photocurrent.

From the above-mentioned experiment results, using an undoped n^- -GaN layer with a lower dislocation density is obviously necessary to achieve a higher responsivity in the GaN Schottky barrier photodetectors. In addition, the unexpected decrease in measured responsivity are observed in a specific GaN Schottky barrier photodetector at high reverse bias voltage (Zhang et al., 2008). A model is proposed which explains the phenomena and suggests that the choice of load resistance is also important for the application of GaN UV photodetectors.

2.2.4 Fabrication of GaN avalanche photodiodes

In this section, the fabrication and characterization of GaN-based p-i-n avalanche photodiodes (APD) with large active area are discussed (Liu et al., 2009), which is suitable

for the very weak ultraviolet radiation detection. The cross section and plan view schematic diagrams of a typical GaN p-i-n APD are shown in Fig.13. A 350nm thick SiO₂ layer was deposited on the mesa surface by plasma enhanced chemical vapor deposition (PECVD) to protect the mesa and to passivate the damage induced by dry etching. A Ni (5nm)/Au (5nm) p-contact layer was formed by electron-beam evaporation and lift-off, then Ti/Al/Ti/Au (15nm/250nm/50nm/150nm) multilayer contact layers were evaporated on both n-type layer serving as an Ohmic electrode and thin Ni/Au contact as a top interconnect pad.

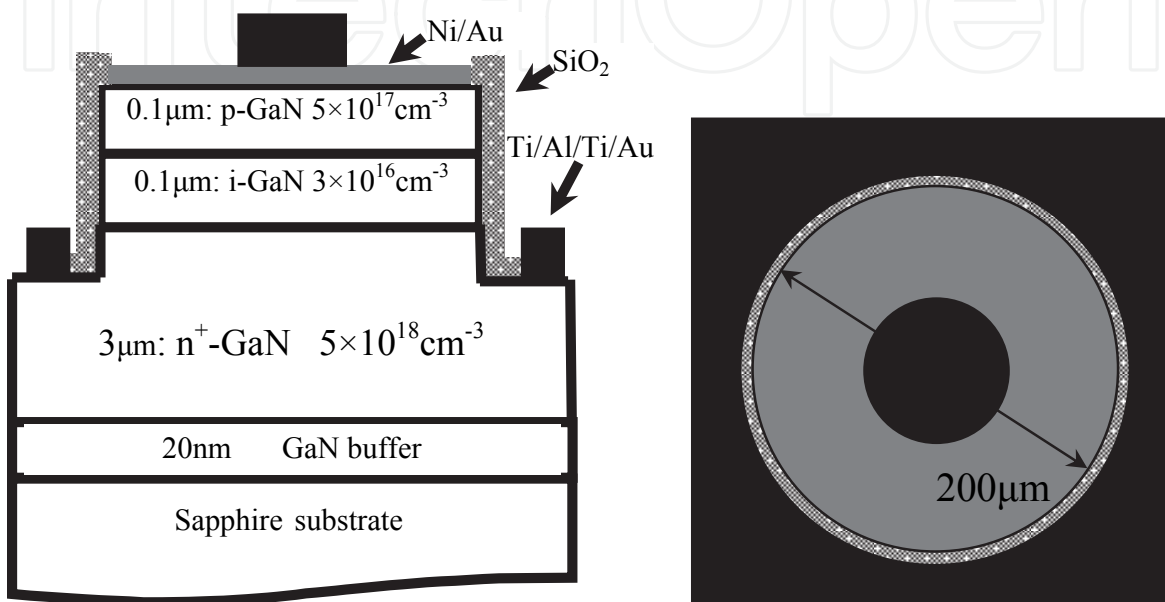


Fig. 12. The cross section and plan view schematic diagrams of the GaN APD

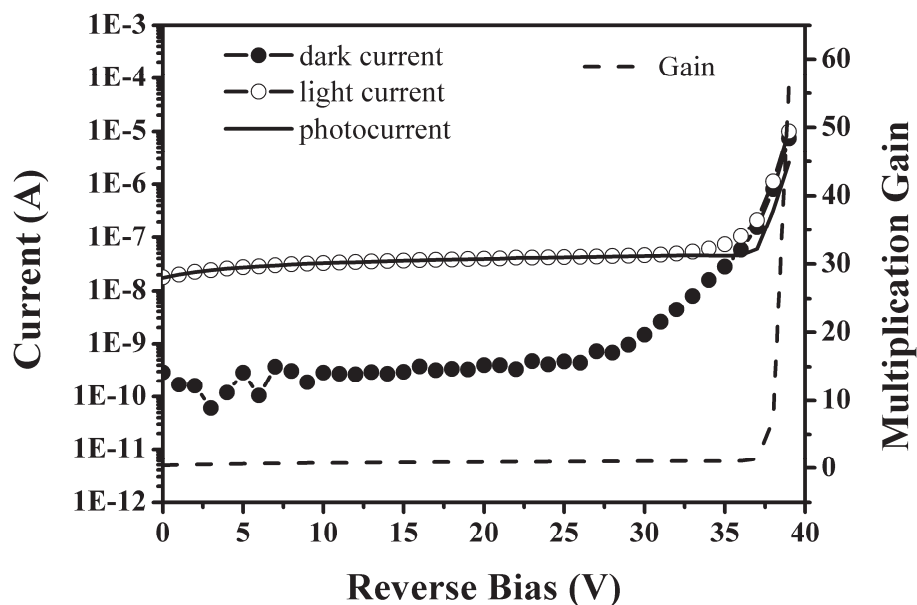


Fig. 13. The dark current and light ($\lambda=360\text{nm}$) current measured in the APD with large device area. The solid line represents the calculated photocurrent. The right-hand axis indicates the normalized gain with the unity gain at -35V as shown by dashed line.

The solid circles in Fig. 13 shows the current voltage (I-V) characteristics in dark at room temperature. The dark current for 200 μm -diameter devices with the reverse bias smaller than 20V was on the order of ~ 0.05 nA, which is down to the measurement limit of Keithly 2400 sourcemeter. This very low leakage current of GaN APD with relatively large area was ascribed to the low defect density of the material [The FWHM values of both (0002) and (10-12) XRD were found to be as narrow as ~ 200 arcsec, the density of screw and edge dislocations is estimated to be about $8 \times 10^7 \text{ cm}^{-2}$ and $7.3 \times 10^7 \text{ cm}^{-2}$, respectively.], as well as the low plasma-induced etch damage of the mesa and the high quality of dielectric passivation. The dark current exhibits a sudden increase at about -38V, as shown in Fig. 14, indicating that the device reaches avalanche breakdown. It means that the impact ionization across the band gap occurs under the high electric field in the depletion region of p-n junction. This process is nondestructive for device. We can prove the reproducibility by performing many times of I-V scan. The breakdown behaviors of the device can be repeated with nearly the same leakage current and the consistent breakdown voltage characteristics. Therefore, the sidewall or local breakdown which may degrade the device is effectively eliminated. Under reverse bias stress near breakdown no light emission from dispersed spots induced by microplasmas was observed. It suggested that the breakdown was uniform in the device. The maximal electric field at the onset avalanche breakdown voltage ($V_b = -38\text{V}$) was estimated to be about 2.9 MV/cm. We attribute this high breakdown field to the optimized growth conditions and the sophisticated device fabrication process which are able to give rise to the uniform breakdown over the entire junction area.

The light current of APD was measured under $\lambda = 360\text{nm}$ illumination. As shown in Fig. 13, it is found that the photocurrent (the difference between light current and dark current represented by the curves with hollow circles and solid circles, respectively) takes only very little variation until the device reaches breakdown at high reverse voltage. If the reverse bias increases beyond 38V, the photocurrent increases dramatically. In the obtained light current curves no any significant change is observed even several times of I-V scan are performed, demonstrating a stable multiplication gain of the avalanche process. Then the avalanche gain can be taken by normalizing the photocurrent with setting the low bias flat region as the unity photocurrent gain. Finally the p-i-n APD with a large device area of 200 μm -diameter has shown a stable avalanche multiplication gain larger than 57 at a reverse bias of 39V. We can conclude that with optimized fabrication procedures (controlled defects density of wafer, suitable structural design, and sophisticated device process), uniform bulk breakdown and stable avalanche multiplication gain can be achieved in APDs with large area grown on c-plane sapphire substrates by MOCVD.

2.2.5 New structure GaN UV photodetectors

An interesting device structure of GaN photodetectors which can be used for judging the wavelength of incident ultraviolet light is proposed (Zhao et al., 2008b). The device structure is composed of two back-to-back conventional GaN UV photodiodes with very different spectral response between 240 and 360 nm. The wavelength of incident light can be identified by measuring the photocurrent ratio of these two photodiodes, which is not dependent on the incident light power, but just strongly dependent on its wavelength.

Fig. 14(a) shows the schematic diagram of the proposed GaN photodetector structure. It is composed of two integrated back-to-back photodiodes, one with *p-n* and another with *p-i-n* structure. The first photodiode (PD_1), a *p-n* GaN structure, consists of electrode 1, n^- -GaN

layer 1, p -GaN layer and electrode 2. The second photodiode (PD_2) is a p - i - n GaN structure, which consists of electrode 2, p -GaN layer, n^- -GaN layer 2 (i -GaN layer), n^+ -GaN layer, and electrode 3. The photosensitive area of PD_1 and PD_2 is nearly the same when the incident light illuminates the semitransparent electrode of the front side of the device, as shown in Fig. 14(a). The characteristics of the two photodiodes and the electrode transmittance function are calibrated in a preliminary step as they will play a part in the measurements to be performed. The equivalent circuit of the device is shown in Fig. 14(b). Obviously PD_1 and PD_2 form an integrated back-to-back structure. The spectral response of these two photodiodes is simulated, and the designed structural parameters for PD_1 are as follows: the top n^- -GaN layer 1 and the p -GaN layer are $0.2\mu\text{m}$ and $0.3\mu\text{m}$, respectively, while the carrier concentrations of n^- -GaN layer 1 and p -GaN layer are $1\times 10^{16}\text{cm}^{-3}$ and $5\times 10^{17}\text{cm}^{-3}$, respectively. The spectral response of PD_1 is shown by the solid line in the inset of Fig. 15. It is seen that the quantum efficiency of PD_1 (QE_1) only slightly decreases with the decrease of wavelength. It is worthwhile noticing that the carrier concentration of the p -GaN layer is relatively high and the doping concentration of the n^- -GaN layer 1 is low in the designed structure. The latter layer is completely depleted, even when there is a low Schottky barrier between the electrode 1 and n^- -GaN layer 1. As a result, the electric field in the n^- -GaN layer is so strong that most of photo-generated electron-hole pairs can be swiftly swept out and contribute to the photocurrent even when the absorption is stronger in the shorter wavelength region. Namely the PD_1 is not much influenced by the surface states. Therefore, the spectral response of PD_1 is quite flat in the wavelength region between 360 and 240 nm.

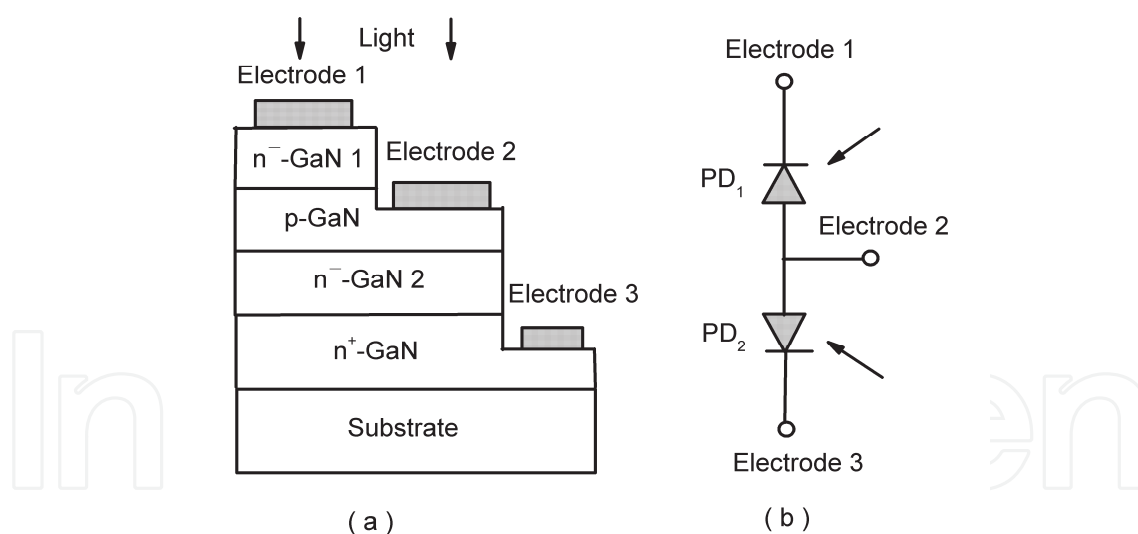


Fig. 14. (a) The schematic diagram of the structure for proposed wavelength-characterizing GaN photodetector; (b) The equivalent circuit of the proposed GaN photodetector

The spectral response of PD_2 is different from that of PD_1 . The design of structure parameters of PD_2 is as follows: the n^- -GaN layer 2 and the p -GaN layer are $0.3\mu\text{m}$ and $0.2\mu\text{m}$, respectively. The carrier concentrations of n^- -GaN layer 2, n^+ -GaN layer and p -GaN layer are $1\times 10^{16}\text{cm}^{-3}$, $5\times 10^{18}\text{cm}^{-3}$ and $5\times 10^{17}\text{cm}^{-3}$, respectively. As shown by the dashed line in Fig. 15, it is found that the quantum efficiency of PD_2 (QE_2) decreases rapidly with the decrease of wavelength. We can explain the phenomenon as follows: the absorption

coefficient above the band gap of GaN is as high as in the order of 10^5 cm^{-1} , the penetration depth is smaller than $0.2 \mu\text{m}$ in the short-wavelength region (Zhao et al., 2006e). The depletion region is distributed mainly on the side of n^- -GaN layer 2 instead on the p -GaN side. Therefore, most of photo-generated carriers in p -GaN layer must diffuse to the electric field region (or depletion region) before they can contribute to the photocurrent. When the wavelength of incident light becomes shorter, the absorption of GaN becomes larger, and most of photons are absorbed by the p -GaN layer. A large part of photo-generated carriers in the p -GaN layer recombine before they reach the depletion region. So the quantum efficiency of the p - i - n GaN ultraviolet photodiode decreases rapidly with the decrease of wavelength, as shown in the inset of Fig.16 by the dashed line.

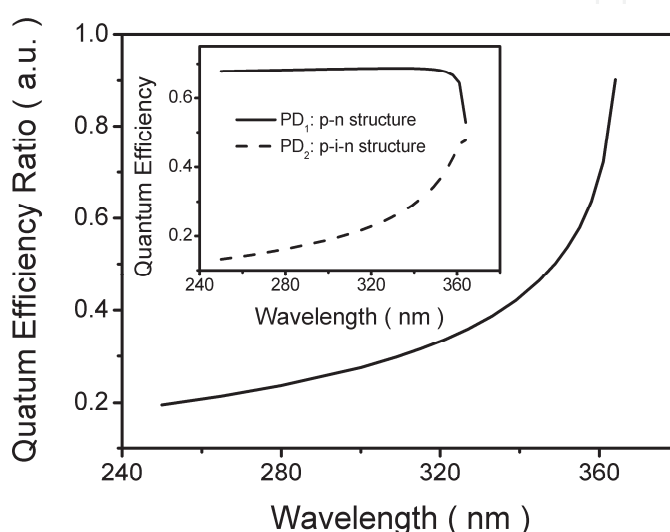


Fig. 15. The ratio of quantum efficiency of PD_2 to PD_1 (QE_2/QE_1) vs. wavelength of incident ultraviolet light. The inset shows the simulated spectral responses of PD_1 and PD_2 which are shown by the solid line and dashed line, respectively.

It is noted that for the proposed GaN device, the designed spectral response of PD_1 and PD_2 must be very different. The spectral response of PD_1 is flat while the slope of spectral response of PD_2 is much steeper, the latter should be dependent on the wavelength as much as possible. It is why PD_1 is a p - n structure while PD_2 is a p - i - n structure. For PD_2 , the thickness and doping concentration of the p -GaN layer are carefully chosen. This layer is relatively thick and has a higher carrier concentration to ensure that a large part of the p -GaN layer is not depleted. Instead, the n^- -GaN layer 2 has a lower doping concentration. Therefore the main part of n^- -GaN layer 2 is a depletion region with strong electric field. Actually, most of incident photons are absorbed by the un-depleted p -GaN layer region and then arrive to the n^- -GaN layer 2 by diffusion to form photocurrent at the junction. However, the p -GaN layer should not be too thick, otherwise a lot of photo-generated carriers will not be able to reach the n^- -GaN layer 2 by diffusion, leading to a low quantum efficiency of PD_2 . There is an electric circuit employed to measure the quantum efficiency ratio of PD_1 to PD_2 (Zhao et al., 2008). After two logarithm circuits and a subtraction circuit, the quantum efficiency ratio of PD_2 to PD_1 could be obtained (Kato et al., 1983), then the wavelength of incident light can be determined, since the quantum efficiency ratio of these two photodiodes is strongly dependent on the wavelength but not on the power of incident light.

In addition, A new structure of GaN based Schottky barrier ultraviolet photodetector is proposed, in which a thin n-type AlGa_N window layer is added on the conventional n⁻-Ga_N/n⁺-Ga_N device structure (Zhou & Zhao, 2007). The simulation result shows that the new structure can reduce the negative effect of surface states on the performance of Schottky barrier GaN photodetectors and then improve the performance. It is also found that an N-face growth structure can improve the quantum efficiency while a Ga-face structure may cause the decrease of quantum efficiency near the band-edge energy of p-i-n heterostructure UV photodetector (Li et al., 2004). In addition, a new method to estimate the hole concentration of p-type GaN by analyzing the spectral response of p-n⁺ GaN UV photodetectors is suggested (Zhao et al., 2010b). It is demonstrated that the device simulation is very helpful for the fabrication and designing of new structures of GaN UV photodetectors.

3. Conclusion

In summary, both GaN materials and III-nitrides based UV photodetectors have been introduced. In the aspect of GaN and AlGa_N materials, the growth mechanism and the yellow luminescence band related defects are investigated. In the aspect of GaN UV photodetectors, the fabrication and performances of Schottky barrier photodetectors, and the fabrication and characterization of p-i-n structure APDs are studied. We hope all these contents may be helpful for the readers and accelerate the development of GaN ultraviolet photodetectors.

4. Acknowledgment

The authors acknowledge the support from the National Science Fund for Distinguished Young Scholars (Grant No. 60925017), the National Natural Science Foundation of China (Grant Nos. 10990100, 60836003 and 60776047), and the National High Technology Research and Development Program of China (Grant Nos. 2007AA03Z401, 2004AA31G240 and 2001AA313050).

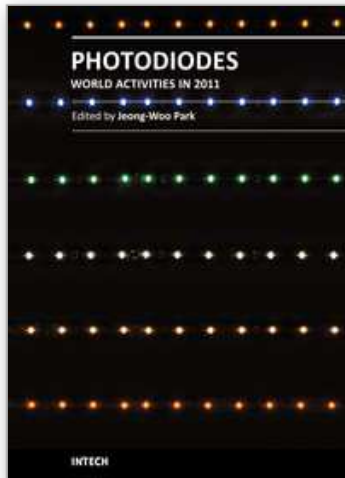
5. References

- Amano H., Sawaki N., Akasaki I., and Toyoda Y. (1986). *Applied Physics Letters*, Vol. 48, No.5, pp.353-355
- Cicek E., Vashaei Z., McClintock R., Bayram C., Razeghi M. (2010). *Applied Physics Letters*, Vol. 96, No.26, p.261107
- Deng Y., Zhao D. G., Le L. C., Jiang D. S., Wu L. L., Zhu J. J., Wang H., Liu Z. S., Zhang S. M., Yang H., and Liang J. W. (2011). *Journal of Alloys and Compounds*, Vol.509, No.3, pp.748-750.
- Han J., Ng T. B., Biefeld R. M., Crawford M. H., and Follstaedt D. M. (1997). *Applied Physics Letters*, Vol. 71, No.21, pp.3114-3116.
- Heinke H., Kirchner V., Einfeldt S., and Hommel D. (2000). *Applied Physics Letters*, Vol.77, No.14, pp.2145-2147.
- Heying B., Wu X. H., Keller S., Li Y., Kopolnek D., Keller B. P., DenBaars S. P., and Speck J. S. (1996). *Applied Physics Letters*, Vol.68, No.5, pp.643-645.

- Kato H., Kojima M., and Yoshida A. (1983). *Review of Scientific instruments*, Vol.54, No.6, pp.728-732.
- Krtschil A., Dadgar A., and Krost A. (2003). *Applied Physics Letters*, Vol.82, No.14, pp.2263-2265.
- Li N., Zhao D. G. and Yang H. (2004). *Solid State Communication*, Vol.132, No.10, pp.701-705.
- Liu W. B., Zhao D. G., Sun X., Zhang S., Jiang D. S., Wang H., Zhang S. M., Liu Z. S., Zhu J. J., Wang Y. T., Duan L. H. and Yang H. (2009). *Journal of Physics D: Applied Physics*, Vol.2, No.1, p.015108.
- Look D. C. and Sizelove J. R. (1999). *Physical Review Letters*, Vol.82, No.6, pp.1237-1240.
- McClintock R., Mayes K., Yasan A., Shiell D., Kung P., Razeghi M. (2005). *Applied Physics Letters*, Vol.86, No.1, p.011117
- Mihopoulos T. G., Gupta V., and Jensen K. F. (1998). *Journal of Crystal Growth*, Vol.195, No.1-4, pp.733-739.
- Muñoz E., Monroy E., Pau J. L., Calle F., Omnès F., and Gibart P. (2001). *Journal of Physics: Condensed Matter*, Vol.13, No.32, pp.7115-7137
- Nakamura K, Makino O, Tachibana A, Matsumoto K. (2000). *Journal of Organometallic Chemistry*, Vol611, No.1-2, pp.514-524.
- Nakamura S. (1991). *Japanese Journal of Applied Physics*, Vol. 30, No. 10A, pp.L1705-L1707
- Nakamura S. (1998). *Science*, Vol.281, No.5379, pp. 956-961
- Ng H. M., Doppalapudi D., Moustakas T. D., Weimann N. G., Eastman L. F. (1998). *Applied Physics Letters*, Vol.73, No.6, pp.821-823.
- Jain S. C., Willander M., Narayan J., and Van Overstraeten R. (2000). *Journal of Applied Physics*, Vol.87, p.965-1006
- Podor B. (1966). *Physica Status Solidi*, Vol.16, No.2, p.K167.
- Reshchikov M. A. and Morkoc H. (2005). *Journal of Applied Physics*, Vol.97, No.6, p.061301.
- Read W. T. (1954). *Philosophical Magazine*, Vol.45, No.367, pp.775-796
- Wu J., Walukiewicz W., Yu K. M., Ager J. W., Haller E. E., Lu H., Schaff W. J., Saito Y., Nanishi Y. (2002). *Applied Physics Letters*, Vol.80, No.21, pp.3967-3969
- Zhang J. P., Khan M. A., Sun W. H., Wang H. M., Chen C. Q., Fareed Q., Kuokstis E., and Yang J. W. (2002). *Applied Physics Letters*, Vol.81, No.23, pp.4392-4394.
- Zhang S., Zhao D. G., Jiang D. S., Liu W. B., Duan L. H., Wang Y. T., Zhu J. J., Liu Z. S., Zhang S. M., and Yang H. (2008). *Semiconductor Science and Technology*, Vol.23, No.10, p.105015.
- Zhao D. G., Zhu J. J., Liu Z. S., Zhang S. M., Yang H. and Jiang D. S. (2004). *Applied Physics Letters*, Vol. 85, No. 9, pp. 1499-1501
- Zhao D. G., Yang H., Zhu J. J., Jiang D. S., Liu Z. S., Zhang S. M., Wang Y. T., and Liang J. W., (2006a). *Applied Physics Letters*, Vol.89, No.11, p.112106.
- Zhao D. G., Zhu J. J., Jiang D. S., Yang H., Liang J. W., Li X. Y., and Gong H. M. (2006b). *Journal of Crystal Growth*, Vol.289, No.1, pp.72-75.
- Zhao D. G., Liu Z. S., Zhu J. J., Zhang S. M., Jiang D. S., Yang H., Liang J. W., Li X. Y., and Gong H. M. (2006c). *Applied Surface Science*, Vol.253, No. pp. 2452.
- Zhao D. G., Jiang D. S., Yang H., Zhu J. J., Liu Z. S., Zhang S. M., Liang J. W., Li X., Li X. Y., and Gong H. M. (2006d). *Applied Physics Letters*, Vol.88, No.24, p.241917.
- Zhao D. G., Jiang D. S., Yang H., Zhu J. J., Liu Z. S., Zhang S. M., Liang J. W., Hao X. P., Wei L., Li X., Li X. Y., and Gong H. M. (2006e). *Applied Physics Letters*, Vol.88, No.25, p.252101.

- Zhao D. G., Jiang D. S., Zhu J. J., Liu Z. S., Zhang S. M., Liang J. W., Yang H., Li X., Li X. Y., Gong H. M. (2007a). *Applied Physics Letters*, Vol.90, No.6, p.062106.
- Zhao D. G., Jiang D. S., Zhu J. J., Liu Z. S., Zhang S. M., Yang H. and Liang J. W. (2007b). *Journal of Crystal Growth*, Vol. 303, No. 2, pp.414-418.
- Zhao D. G., Jiang D. S., Zhu J. J., Liu Z. S., Zhang S. M., Liang J. W. and Yang H. (2007c) . *Journal of Applied Physics*, Vol.102, No. 11, p.113521.
- Zhao D. G., Jiang D. S., Zhu J. J., Liu Z. S., Zhang S. M., Yang H., Jahn U., and Ploog K. H. (2008a). *Journal of Crystal Growth*, Vol.310, No.24, pp.5266-5269.
- Zhao D. G., Jiang D. S., Zhu J. J., Liu Z. S., Zhang S. M. and Yang H. (2008b). *Semiconductor Science and Technology*, Vol.23, No.9, p.095021.
- Zhao D. G., Jiang D. S., Zhu J. J., Guo X., Liu Z. S., Zhang S. M., Wang Y. T., and Yang H. (2009a). *Journal of Alloys and Compounds*, Vol.487, No.1-2, p.400-403.
- Zhao D. G., Jiang D. S., Zhu J. J., Liu Z. S., Wang H., Zhang S. M., Wang Y. T., and Yang H. (2009b). *Applied Physics Letters*, Vol.95, No.4, p. 041901.
- Zhao D. G., Zhang S., Liu W. B., Hao X. P., Jiang D. S., Zhu J. J., Liu Z. S., Wang H., Zhang S. M., Yang H., and Wei L. (2010a). *Chinese Physics B*, Vol.19, No.5, p.057802.
- Zhao D. G., Jiang D. S., Zhu J. J., Wang H., Liu Z. S., Zhang S. M., and Yang H. (2010b). *Journal of Alloys and Compounds*, Vol.492, No.1-2, p.300-302.
- Zhou M. and Zhao D. G. (2007). *Chinese Physics Letters*, Vol.24, No.6, pp.1745-1748.

IntechOpen



Photodiodes - World Activities in 2011

Edited by Prof. Jeong Woo Park

ISBN 978-953-307-530-3

Hard cover, 400 pages

Publisher InTech

Published online 29, July, 2011

Published in print edition July, 2011

Photodiodes or photodetectors are in one boat with our human race. Efforts of people in related fields are contained in this book. This book would be valuable to those who want to obtain knowledge and inspiration in the related area.

How to reference

In order to correctly reference this scholarly work, feel free to copy and paste the following:

D. G. Zhao and D. S. Jiang (2011). GaN Based Ultraviolet Photodetectors, Photodiodes - World Activities in 2011, Prof. Jeong Woo Park (Ed.), ISBN: 978-953-307-530-3, InTech, Available from:
<http://www.intechopen.com/books/photodiodes-world-activities-in-2011/gan-based-ultraviolet-photodetectors>

INTECH
open science | open minds

InTech Europe

University Campus STeP Ri
Slavka Krautzeka 83/A
51000 Rijeka, Croatia
Phone: +385 (51) 770 447
Fax: +385 (51) 686 166
www.intechopen.com

InTech China

Unit 405, Office Block, Hotel Equatorial Shanghai
No.65, Yan An Road (West), Shanghai, 200040, China
中国上海市延安西路65号上海国际贵都大饭店办公楼405单元
Phone: +86-21-62489820
Fax: +86-21-62489821

© 2011 The Author(s). Licensee IntechOpen. This chapter is distributed under the terms of the [Creative Commons Attribution-NonCommercial-ShareAlike-3.0 License](https://creativecommons.org/licenses/by-nc-sa/3.0/), which permits use, distribution and reproduction for non-commercial purposes, provided the original is properly cited and derivative works building on this content are distributed under the same license.

IntechOpen

IntechOpen